



AIAA 2003-1321

**A Robust Statistical Model for the
Evaporation of Multicomponent-Fuel
Drops Containing a Multitude of
Chemical Species**

K. G. Harstad, P. C. Le Clercq and J. Bellan
Jet Propulsion Laboratory
California Institute of Technology
Pasadena, CA

**41st AIAA Aerospace Sciences
Meeting & Exhibit**

6-9 January 2003/ Reno, NV

**For permission to copy or to republish, contact the copyright owner named on the first page.
For AIAA-held copyright, write to AIAA Permissions Department,
1801 Alexander Bell Drive, Suite 500, Reston, VA, 20191-4344.**

A Robust Statistical Model for the Evaporation of Multicomponent-Fuel Drops Containing a Multitude of Chemical Species¹

K. G. Harstad*, P. C. Le Clercq** and J. Bellan***²

Jet Propulsion Laboratory
California Institute of Technology
Pasadena, CA 91109-8099

Abstract

A statistical formulation is developed describing the composition in an evaporating multicomponent-fuel liquid drop and in the gas phase surrounding it. The initial fuel composition is specified by a Gamma Probability Distribution Function (PDF) according to Continuous Thermodynamics (CT) results. Using a discrete-component model and the classical quasi-steady gas phase assumption with respect to the liquid, it is shown that when drops are immersed in a carrier gas containing fuel vapor, condensation of species onto the drop results in the development of a minor peak in the liquid composition PDF. This peak changes the mathematical form of the PDF to a shape that can be viewed as a superposition of two Gamma PDFs. Based on such a superposition of two Gamma PDFs, called the double- Γ -PDF, and using CT concepts combined with the quasi-steady gas phase assumption, a model is developed for calculating the parameters of the double- Γ -PDF. Extensive tests of the model for diesel fuel show that the double- Γ -PDF results replicate accurately the discrete model predictions. Most important, the mean and variance of the composition at the drop surface, which determine the gas phase composition, are in excellent agreement with the discrete model. Results from the model show that although the second peak is minor for the liquid PDF, its corresponding peak for the vapor distribution at the drop surface has a comparable magnitude to and sometimes exceeds that which corresponds to the first peak.

Introduction

The modeling of multicomponent drop evaporation is a challenging task owing to the difficulty in portraying the coupled behavior of a multitude of chemical species. Detailed models of multicomponent-fuel (MC-fuel) drops were developed more than twenty years ago by [1] and [2] but were considered impractical to use in sprays since the computation time was prohibitive even for a single drop composed of a three species mixture. Even with current

computational capabilities, the calculation time remains daunting if many millions of drops must be considered, as in any practical spray application. To mitigate this situation, it was proposed [3] to replace the complex MC-fuel mixture by a binary mixture composed of an effective solvent and an effective solute chosen according to a rigorous criterion following the needs of the application. This model yielded a very efficient computer code, and introduced a new non-dimensional number that characterized the drop regime evaporation according to the dominance of the solvent or solute. Simulations conducted for dilute (i.e. small drop number density) clusters of drops recovered the isolated drop experiment-based paradigm proposed by [4]. Results from dense drop clusters showed deviations from the single drop behavior due to the substantial effect of drop interactions. However, by construct the model could not be applied to the more general situation where there is neither a well-defined solvent nor a solute, and could not account for the entire range of species constituting a realistic fuel composition.

Most experiments of single real-fuel drops suffer from difficulties in measuring the fuel composition from the initial condition up to the drop disappearance. The problem is that current measurement techniques cannot capture the drop composition during the initial heating transients even for drops composed of a binary species mixture [5] [6] [7], and so it is only the D^2 history, where D is the drop diameter, that is documented [6] [8] [9] [10] [11] [12]. This means that the presented $D^2(t)$, where t denotes the time, documents a drop whose initial composition is unknown since differential evaporation of the species occurs during the heat up time. Sometimes, drop temperature measurements are available either at the surface [13] or more seldom inside the drop [14]. In the following, we will show that drop temperature information is not a reliable indicator of its chemical composition.

This study is devoted to the modeling of MC-fuel drops containing a very large number of species. Such a model was proposed by [15] and [16], and utilized by [17] and [18]. This model is based on a statistical representation of the fuel composition using Continuous Thermodynamics (CT). CT is a theory [19] [20] [21] [22] [23] in which the composition of a mixture is described by a probability distribution function (PDF) rather than by a series of discrete values of the concentration. Generally, this PDF is a function of all thermophysical properties of the chemical

¹ Copyright © 2003 by the California Institute of Technology, published by the American Institute of Aeronautics and Astronautics, Inc., with permission. All rights reserved.

² *Senior Engineer; **Postdoctoral Fellow, *** Senior Research Scientist, AIAA Associate Fellow (corresponding author, josette.bellan@jpl.nasa.gov).

species, however, in practical applications it can be chosen to depend on one or several properties of interest of the mixture [22] such as the relative volatility [19], the normal boiling point, the number of carbon atoms per molecule, or most conveniently for many applications, the molar weight [23]. The simplification that the PDF depends only on the molar weight is possible for mixtures composed of homologous species [24] [23] and such distributions, based on the Gamma PDF (Γ -PDF), are available for diesel fuel, gasoline and kerosene [23] [15]. Thus, the advantage of CT theory is that the mixture composition can be represented by a small number of parameters rather than by the prohibitively large number of parameters that would be necessary even for a discretely described surrogate fuel. The theory is based on the appropriate representation of the chemical potential for a mixture containing numerous components and uses molecular thermodynamic methods to represent the Gibbs function in terms of this PDF. The concepts are fundamental and independent of the physico-chemical model chosen to represent the chemical potential.

However the drop model based on the Γ -PDF [15] [16] turned out to have some deficiencies, as reported by [17]. Specifically, unphysical results were obtained for drops evaporating in gas vitiated with fuel vapor, or for large evaporation rates. The goal of this investigation is to formulate a model that is also based on statistical concepts, but that is more robust. Since measurements are not available for testing the model, the results from a discrete species model are considered to provide the ‘exact’ distribution that must be replicated by the model. The proposed statistical model is evaluated by performing tests with diesel fuel under a wide range of conditions. The assessment of the model is summarized in the concluding remarks.

Models of multicomponent drop evaporation

In any model, physical accuracy must be balanced against complexity. Aiming at a drop model that is usable in configurations where there are millions of drops, the goal is to develop a model that captures the crucial features of the MC-fuel but that is simple enough to be one of the building blocks of a larger model. Therefore, several assumptions are made, as follows: The drop is spherical of radius R . The liquid has a constant density ρ_l . Liquid evaporation is assumed to occur under thermodynamic equilibrium. The carrier gas surrounding the drop, denoted by the subscript a , obeys the perfect gas equation of state. The gas is postulated to be quasi-steady with respect to the liquid, which is justified by its much smaller characteristic time compared to that of the liquid. Furthermore, we are only interested in the average volumetric properties of the drop represented by its temperature T_d , and mass fractions of different species, $Y_{il} = M_i/M_d$, where $M_d = 4\pi R^3 \rho_l/3$ is the drop mass and the liquid is a mixture of N species i of individual mass M_i inside the drop, $\sum_{i=1}^N M_i = M_d$. The interest in average drop properties precludes consideration of differential species diffusivities, and therefore of

any phenomena resulting from such processes. The study is performed at atmospheric pressure where solubility of the carrier gas into the liquid is negligible and the far field conditions are assumed quiescent.

The discrete-species drop model

A discrete representation of the mixture composition as a function of the molar weight is shown in Fig. 1a. The idea is to create ‘bins’ in the molar weight space and represent the mixture by these species or pseudo-species.

Liquid phase conservation equations

The conservation equations for mass, species and the energy are:

$$\frac{dM_d}{dt} = -\dot{m}, \quad (1)$$

$$\frac{dM_i}{dt} = Y_{il} \frac{dM_d}{dt} - 4\pi R^2 j_{il}^{(s)} \quad (2)$$

$$\frac{4\pi R^3}{3} \rho_l C_l \frac{dT_d}{dt} = 4\pi R^2 \left(-q_l^{(s)} + \sum_{j=1}^N (h_{jl} - h_{al}) j_{jl}^{(s)} \right) \quad (3)$$

where \dot{m} is the evaporation rate, $j_{il}^{(s)}$ and $q_l^{(s)}$ are the species mass and heat flux at the drop surface on the liquid side, h_{jl} is the enthalpy of the species j in the liquid and h_{al} is the enthalpy of the carrier gas in the liquid. The assumption that solubility effects are negligible imply that $(h_{ag} - h_{al}) \simeq 0$ where h_{ag} is the enthalpy of the carrier gas in the gas phase. This is a set for $N+2$ equations and same number of unknowns: M_d , Y_{il} and T_d .

Gas phase conservation equations

The conservation equations for mass, species and energy are:

$$\frac{d(\rho_g u_g r^2)}{dr} = 0, \quad (4)$$

$$\rho_g u_g r^2 \frac{dY_{jg}}{dr} = -\frac{d}{dr} (r^2 j_{jg}), \quad j \in \{[1, N], a\}, \quad (5)$$

$$\rho_g u_g r^2 C_p \frac{dT_g}{dr} = \sum_{j=1}^N (h_{jg} - h_{ag}) \frac{d}{dr} (r^2 j_{jg}) - \frac{d}{dr} (r^2 q_g), \quad (6)$$

augmented by the equation of state

$$p = \rho_g \tilde{R} T_g, \quad (7)$$

where r is the radial coordinate, ρ_g is the gas density, u_g is the gas velocity, Y_{jg} is the mass fraction of species j in the gas, T_g is the gas temperature and p is the pressure. Generally, the gas is composed of the N species of the liquid, now in gaseous phase, and the carrier gas which may be a mixture of several species conveniently assembled as a pseudo-species and distinguished from the evaporated species. The ensemble of the evaporated species is called the vapor and denoted by the subscript v . $\tilde{R} = R_u \sum_j Y_{jg}/m_j$ is the gas constant, where R_u is the universal gas constant and

m_j is the molar weight of species j . h_{ig} is the enthalpy of the fuel species i in the gaseous phase. According to [25], the gaseous fuel species mass fluxes and the heat flux are:

$$j_{jg} = -\rho_g \sum_{k=1}^N \mathcal{D}'_{jk} \frac{dY_{kg}}{dr} \quad (8)$$

$$q_g = -\lambda_g \frac{dT_g}{dr} + \sum_{i=1}^N (h_{ig} - h_{ag}) j_{ig}, \quad (9)$$

where

$$\mathcal{D}'_{jk} = \frac{m_j}{m_k} [\mathcal{D}_{jk} - (1 - \frac{m_k}{m_a}) \bar{\mathcal{D}}_j], \quad \bar{\mathcal{D}}_j \equiv \sum_k \mathcal{D}_{jk} X_{kg}, \quad (10)$$

with X_{kg} being the mole fraction and $\mathcal{D}_{ik} = (\delta_{ik} - \delta_{ia}) \sum_j D_{m,ij} (m_j/m) Y_j - Y_i (m_k D_{m,ik} - m_a D_{m,ia}) / m$, where $m = \sum_j m_j X_j$ and δ is the Dirac delta function. The symmetric matrix $D_{m,ij}$, which represents the diffusion coefficients, is related to the Fick's diffusion elements in the transport matrix [26], L_{ij} , through $L_{ij} \equiv -D_{m,ij} n Y_i Y_j$, $i \neq j$ where n is the molar density. There are therefore $N + 3$ unknowns (Y_{jg} , u_g , ρ_g and T_g) and the same number of equations (Eqs. 4, 5, 6 and 7) since p is specified and is independent of r .

Boundary conditions

There are two locations where boundary conditions apply: the gas far field and the drop surface. In the far field, the values of the mass fractions, the temperature and the pressure are prescribed: $Y_{jg}^{(\infty)}$, $T_g^{(\infty)}$ and $p^{(\infty)}$. At the drop surface, there is conservation of the mass-species and heat fluxes, and the Clausius-Clapeyron law governs the phase change under vapor-liquid equilibrium at the surface.

The conservation of species mass flux at the drop surface is

$$4\pi R^2 j_{il}^{(s)} + \dot{m} Y_{il} = 4\pi R^2 j_{jg}^{(s)} + \dot{m} Y_{jg}^{(s)} \text{ for } i \in [1, N], \quad (11)$$

$$0 = 4\pi R^2 j_{ag}^{(s)} + \dot{m} Y_{ag}^{(s)}, \quad (12)$$

and the conservation of heat flux at the drop surface is

$$4\pi R^2 q_l^{(s)} = 4\pi R^2 q_g^{(s)} + \dot{m} L_v, \quad (13)$$

where $L_v = h_g^{(s)} - h_l = Y_a^{(s)} h_{ag}^{(s)} + \sum_{i=1}^N (Y_{ig}^{(s)} h_{ig}^{(s)} - Y_{il} h_{il})$ is the mixture latent heat.

The general vapor-liquid equilibrium at the surface of the liquid phase is thermodynamically expressed through the equality of fugacities which at low pressure can be approximated by

$$X_i^{(s)} = X_{il} \left(\mathcal{A}_{il} \frac{p_{sat,i}}{p^{(\infty)}} \right), \quad (14)$$

where $p_{sat} = \sum_j \mathcal{A}_{jl} X_{jl} p_{sat,j}(T)$, \mathcal{A}_{il} is the activity coefficient and $p^{(\infty)}$ is the far field value. Assuming Raoult's law to be valid ($\mathcal{A}_{il} = 1$) yields

$$X_{ig}^{(s)} = X_{il} \frac{p_{sat,i}}{p^{(\infty)}}, \quad Y_{ig}^{(s)} = \frac{m_i}{m_g^{(s)}} X_{ig}^{(s)}, \quad (15)$$

where $m_g^{(s)} = \sum_j m_j X_{jg}^{(s)}$. The species latent heat, $L_{vi}(T) \equiv h_{ig} - h_{il}$, is related to the saturation pressure $p_{sat,i}$ through the Clausius-Clapeyron relation

$$L_{vi}(T) = \frac{R_u T^2}{m_i} \frac{d \ln(p_{sat,i})}{dT}. \quad (16)$$

Since the dependency of the latent heat, $L_{vi}(T)$, on the temperature is weak, it can be estimated at the boiling point and therefore be considered to be function of the molar weight only. Thus, Eq. 16 can be integrated to give

$$p_{sat,i} = p_{atm} \exp \left[\frac{m_i L_{vi}(T=T_{bi})}{R_u T_{bi}} \left(1 - \frac{T_{bi}}{T_g^{(s)}} \right) \right], \quad (17)$$

where T_{bi} is the normal boiling point. We also assume that $T_d = T_g^{(s)}$.

Gas-phase solution within the discrete model

One difficulty in solving the system of equations is that the diffusion coefficients \mathcal{D}'_{ik} are unknown. Whereas these coefficients could in principle be calculated using kinetic theory concepts [27] [28] [29] at this point of theory development they would only introduce an unwarranted complication and serve as a distraction from our goal of developing a simplified statistical mathematical framework for describing multicomponent-fuel drop evaporation. A further simplification is thus introduced by defining an effective average diffusion coefficient, \mathcal{D}_{eff} . With this definition, the traditional solutions for the gas field around a drop are recovered [30]:

$$\frac{dD^2}{dt} = -\frac{8\rho_g^{(s)} \mathcal{D}_{eff}}{\rho_l} \ln(1 + B_m), \quad (18)$$

$$Y_{jg} = \frac{-Y_{jg}^{(\infty)} e^{-Pe} + Y_{jg}^{(s)} + (Y_{jg}^{(\infty)} - Y_{jg}^{(s)}) e^{-zPe}}{(1 - e^{-Pe})}, \quad (19)$$

$$T_g = T_g^{(\infty)} - (T_g^{(\infty)} - T_g^{(s)}) \frac{1 + B_T}{B_T} [1 - (1 + B_T)^{-z}], \quad (20)$$

where $D = 2R$, B_m is the mass Spaulding number [30] defined by $B_m = e^{Pe} - 1$, $Pe \equiv (\rho_g u_g r^2)^{(s)} / (R \rho_g^{(s)} \mathcal{D}_{eff}) = u_g^{(s)} R / \mathcal{D}_{eff}$, $z = R/r$, and B_T is defined by $(1 + B_T) \equiv (1 + B_m)^{1/Le}$ where the Lewis number is $Le \equiv \lambda_g^{(s)} / (C_p^* \rho_g^{(s)} \mathcal{D}_{eff})$. $\lambda_g^{(s)}$ is calculated as a function of $T_g^{(s)}$ using mixing rules (see Appendix 1) and

$$C_p^* = \int_0^1 [C_p(T_g) + \frac{(1 + B_m)^{1-z}}{B_m} \times \sum_i (Y_{ig}^{(s)} - Y_{ig}^{(\infty)}) (C_{p,i} - C_{p,ag})] dz. \quad (21)$$

Using the steady-state profiles from Eqs. 12 and 19 yields $B_m = (Y_v^{(s)} - Y_v^{(\infty)}) / (1 - Y_v^{(s)})$.

To solve the discrete problem, one needs to solve differential equations for D , T_d and Y_{il} , which are called primary variables, and algebraic equations for $q_l^{(s)}$ and $j_{il}^{(s)}$, which are called secondary variables. Therefore there are $N + 2$ primary variables.

Statistics from the discrete model

For a large number of discrete species, one may define the following statistics:

$$\theta_l \equiv \sum_{i=1}^N (m_i X_{il}), \quad \theta_v \equiv \frac{1}{X_v} \sum_{i=1}^N (m_i X_{ig}), \quad (22)$$

$$\xi_{nl} \equiv \sum_{i=1}^N (m_i^n X_{il}), \quad \xi_{nv} \equiv \frac{1}{X_v} \sum_{i=1}^N (m_i^n X_{ig}) \quad (23)$$

where $\theta_l = m_l$, $\theta_v = m_v$, ξ_{nl} and ξ_{nv} are the liquid mean molar weight, the vapor mean molar weight in the gas, the liquid n^{th} moment of the molar weight, the vapor n^{th} moment of the molar weight in the gas, respectively and $X_v \equiv 1 - X_{ag}$. These statistics enable the comparison between results from the statistical models based on a PDF and the discrete model.

These definitions combined with Eqs. 2 also lead to a differential equation for each moment

$$\begin{aligned} \frac{d\xi_{nl}}{dt} = & \frac{3\rho_g^{(s)} \mathcal{D}_{eff} m_l}{\rho_l R^2 m_g^{(s)}} \frac{1 + B_m}{B_m} \ln(1 + B_m) \times \quad (24) \\ & \left[\left(X_v^{(s)} - X_v^{(\infty)} \frac{1 - X_v^{(s)}}{1 - X_v^{(\infty)}} \right) \xi_{nl} \right. \\ & \left. - \left(X_v^{(s)} \xi_{nv}^{(s)} - X_v^{(\infty)} \frac{1 - X_v^{(s)}}{1 - X_v^{(\infty)}} \xi_{nv}^{(\infty)} \right) \right]. \end{aligned}$$

These equations serve as the basis for generalization to the statistical representation presented in our new model.

Continuous thermodynamics using a single- Γ -PDF

The multicomponent droplet vaporization model based on continuous thermodynamics was developed by [15] and [16] and utilized with some revisions by [31] to study temporal mixing layers laden with a multitude of multicomponent-fuel drops. We visualized in Fig. 1b the representation of a mixture composition by the single Γ -PDF.

Description of a mixture using CT theory

In CT form, the mole fraction of a discrete species i is defined by the value of a continuous distribution function, f , in the vicinity of the molar mass point corresponding to that species $X_i = f(m_i) \Delta m_i$. This definition holds for a mixture containing hydrocarbon species only. Such a mixture is, for example, a hydrocarbon liquid fuel such as diesel, gasoline or kerosene for which

$$X_{il} = f_l(m_i) \Delta m_i. \quad (25)$$

For a mixture containing hydrocarbons and non-hydrocarbon species, such distribution functions describing all components are not necessarily available. An example of such a situation is that of gasoline vapor in air. To utilize the CT formulation in this situation, one then

defines the molar fraction of the non-hydrocarbon, here denoted by the subscript ag (ambient carrier gas) and that of the hydrocarbon mixture indexed by v , with $X_{ag} + X_v = 1$, and use the CT formulation for the hydrocarbon as

$$X_{iv} = X_v f_v(m_i) \Delta m_i. \quad (26)$$

Then from the discrete form $m_g = m_{ag} X_{ag} + \sum_{i=1}^N m_i X_{iv}$ one obtains the continuous form

$$m_g = m_{ag}(1 - X_v) + \theta_v X_v \quad (27)$$

where N is the number of species in the fuel and the mean molar weight of the evaporated fuel and the second moment of the distribution are defined as

$$\theta_v = \int_0^\infty f_v(m_i) m_i dm_i, \quad \psi_v = \int_0^\infty f_v(m_i) m_i^2 dm_i. \quad (28)$$

Whitson [32] used the Γ -PDF

$$f_\Gamma(m_i) = \frac{(m_i - \gamma)^{\alpha-1}}{\beta^\alpha \Gamma(\alpha)} \exp\left[-\left(\frac{m_i - \gamma}{\beta}\right)\right] \quad (29)$$

to characterize the high molar-weight portion of crude oils, where $\Gamma(\alpha)$ is the Gamma function. The origin of f is specified by γ , and its shape is determined by two parameters, α and β . These parameters are related to the mean, θ_v , the variance, σ_v^2 , and the second moment, ψ_v , of f by

$$\theta_v = \alpha\beta + \gamma, \quad \sigma_v^2 = \alpha\beta^2, \quad \psi_v = \theta_v^2 + \sigma_v^2. \quad (30)$$

Equations for a single- Γ -PDF

From Eqs. 2 one can derive an equation for the liquid mole fraction:

$$\begin{aligned} \frac{dX_{kl}}{dt} = & \frac{3}{2D^2} \frac{dD^2}{dt} \left(\frac{\theta_l}{Y_v^{(\infty)} - Y_v^{(s)}} \right) \times \quad (31) \\ & \left\{ \left[(1 - Y_v^{(\infty)}) \frac{X_v^{(s)}}{m_g^{(s)}} - (1 - Y_v^{(s)}) \frac{X_v^{(\infty)}}{m_g^{(\infty)}} \right] X_{kl} \right. \\ & \left. - \left[(1 - Y_v^{(\infty)}) \frac{X_{kg}^{(s)}}{m_g^{(s)}} - (1 - Y_v^{(s)}) \frac{X_{kg}^{(\infty)}}{m_g^{(\infty)}} \right] \right\}. \end{aligned}$$

Substituting the discrete mole fractions by their continuous forms (Eqs. 25 and 26) in the vapor and the liquid phases one obtains:

$$\frac{d\theta_l}{dt} = -\frac{3}{2D^2} \frac{dD^2}{dt} \left[\frac{\theta_l^2}{\theta^*} - \theta_l \right], \quad (32)$$

$$\frac{d\psi_l}{dt} = -\frac{3}{2D^2} \frac{dD^2}{dt} \frac{\theta_l}{\theta^*} [\psi_l - \psi^*] \quad (33)$$

where

$$\theta^* = \frac{\mathcal{X}_v^{(s)} \theta_g^{(s)} - \mathcal{X}_v^{(\infty)} \theta_g^{(\infty)}}{(\mathcal{X}_v^{(s)} - \mathcal{X}_v^{(\infty)})}, \quad (34)$$

$$\psi^* = \frac{\mathcal{X}_v^{(s)} \psi_g^{(s)} - \mathcal{X}_v^{(\infty)} \psi_g^{(\infty)}}{(\mathcal{X}_v^{(s)} - \mathcal{X}_v^{(\infty)})}, \quad (35)$$

$$\mathcal{X}_v^{(s)} = \frac{X_v^{(s)}}{1 - X_v^{(s)}}, \quad \mathcal{X}_v^{(\infty)} = \frac{X_v^{(\infty)}}{1 - X_v^{(\infty)}}. \quad (36)$$

Using the CT formulation in conjunction with the conservation equations leads to relationships between the vapor molar fraction at the drop surface, $X_v^{(s)}$, and the distribution parameters in the liquid, and between the distribution parameters in the liquid and vapor

$$X_v^{(s)} = \frac{p_{atm}}{p^{(\infty)}} \frac{\exp\{[\Delta s_{fg}/(R_u T_g^{(s)})](T_g^{(s)} - A_b - \gamma B_b)\}}{\left(1 + [\Delta s_{fg}/(R_u T_g^{(s)})] B_b \beta_l\right)^{\alpha_l}}, \quad (37)$$

$$\theta_v^{(s)} - \gamma = \frac{\theta_l - \gamma}{1 + [\Delta s_{fg}/(R_u T_g^{(s)})] B_b \beta_l}, \quad (38)$$

$$(\sigma_v^{(s)})^2 = \sigma_l^2 \left[\frac{\theta_v^{(s)} - \gamma}{\theta_l - \gamma} \right]^2, \quad (39)$$

having assumed that $\gamma_l = \gamma_v^{(s)} = \gamma$. We also postulate that $T_g^{(s)} = T_d$. In Eqs. 37 - 39, $p_{atm} = 1 \text{ atm}$ and the entropy of evaporation expressed using Trouton's law is $\Delta s_{fg} = m_i L_{vi}/T_{bi} \simeq 87.9 \text{ JK}^{-1} \text{ mol}^{-1}$. The constants A_b and B_b are listed in Appendix 1 and fit $T_b(m_i) = A_b + B_b m_i$.

To solve the problem, one needs to solve for the primary variables D, T_d, θ_l and ψ_l , and for the secondary variables $q_l^{(s)}, j_{jl}^{(s)}, \theta_v^{(s)}, X_v^{(s)}$ and $\psi_v^{(s)}$. There are therefore 4 primary variables, which represents a reduction in number from the $N + 2$ variables of the discrete model; for $N > 2$, it is computationally preferable to use the single- Γ -PDF if the result accuracy is comparable. Once the composition of the mixture is known at the drop surface, Eqs. 19 can be used to find the composition of the gaseous mixture surrounding the drop.

Continuous thermodynamics using a double- Γ -PDF

The deficiencies of the single- Γ -PDF documented in our results comparing its predictions with those of the discrete model displayed in statistical form (see below), prompted our investigation into the description of the fuel molar weight distribution using a superposition of two Γ -PDFs

$$P_l(m_i; \alpha_1, \beta_1, \alpha_2, \beta_2, \epsilon) = (1 - \epsilon) f_{\Gamma}^{(1)}(m_i) + \epsilon f_{\Gamma}^{(2)}(m_i), \quad (40)$$

where $f_{\Gamma}^{(q)}(m_i) = f_{\Gamma}(m_i; \alpha_q, \beta_q)$ with $q \in [1, 2]$, ϵ is a weighing parameter ($0 \leq \epsilon \leq 1$) and $\int_{\gamma}^{\infty} P_l(m_i) dm_i = 1$. The problem of determining P_l can be stated as follows: Given an initial single- Γ -PDF characterized by $\theta_0, \beta_0, \gamma$ and $\epsilon = 0$, is it possible to determine P_l as a function of time? To do so, one needs to solve for the vector $\eta \equiv (\alpha_1, \beta_1, \alpha_2, \beta_2, \epsilon)$ at each time step. We show here that such an approximate solution is possible.

Consider the P_l moments defined by

$$\xi_{nl} \equiv \int_{\gamma}^{\infty} m_i^n P_l(m_i) dm_i \text{ for } n \geq 1. \quad (41)$$

If η is known, ξ_{nl} may be calculated for any value of n . Conversely, an inverse mapping may be defined in that

given ξ_{nl} for $n \in [1, 5]$, η may be calculated. This inverse mapping is the driving idea in determining η .

The differential equations solved for ξ_{nl} are the continuous form of Eq. 24 where the equation is the same except that $m_g^{(s)} = X_v^{(s)} \theta_v^{(s)} + (1 - X_v^{(s)}) m_{ag}$ and m_l is replaced by θ_l . In statistical form, $\xi_{nv}^{(\infty)}$ is specified and by definition

$$\xi_{nv}^{(s)} = \int m_i^n P_v^{(s)}(m_i) dm_i. \quad (42)$$

Raoult's law in continuous form is used to relate the vapor PDF at the drop surface, $P_v^{(s)}$, to $P_l^{(s)}$ and $X_v^{(s)}$ through

$$P_v^{(s)} = \frac{p_{atm}}{X_v^{(s)} p^{(\infty)}} \exp \left[\frac{m_i L_{vi}}{R_u T_{bi}} \left(1 - \frac{T_b(m_i)}{T_d} \right) \right] P_l^{(s)}. \quad (43)$$

Similar to the situation for the single- Γ -PDF, once the composition of the mixture is known at the drop surface, Eqs. 19 can be used to find the composition of the gaseous mixture surrounding the drop.

The form of ξ_{nl} for $n \in [1, 5]$ is calculated as a function of η and is presented elsewhere [33]. By definition, $\xi_{1l} \equiv \theta$ and $\xi_{2l} \equiv \theta^2 + \sigma^2$ and the relationships from Eq. 30 hold. Each ξ_{nl} can be written as

$$\xi_{nl} = (1 - \epsilon) \xi_{nl}^{(1)} + \epsilon \xi_{nl}^{(2)} \quad (44)$$

where $\xi_{1l}^{(j)} = \theta_j$ and $\xi_{2l}^{(j)} = \theta_j^2 + \sigma_j^2$, thus corresponding to the single- Γ -PDF form. Since the double- Γ -PDF can be considered as a departure from the single- Γ -PDF, it is natural to introduce the concept of excess moments, as follows. We define ξ_{nl}^* as being the moments of a single- Γ -PDF that would have the same ξ_{1l} and ξ_{2l} values as a given distribution P_l , and thus $\xi_n' \equiv \xi_{nl} - \xi_{nl}^*$ can be considered to be the departure, or excess, from that form. By definition, $\xi_1' = \xi_2' = 0$ and a double- Γ -PDF then corresponds to $\xi_n' \neq 0$ for $n \geq 3$. Because ξ_{1l} and ξ_{2l} determine θ and σ (or β), the problem of determining η from the moments can thus be further reduced to the inverse map defined by $[\xi_n' \neq 0 \text{ for } n \geq 3 \rightarrow (\theta', \beta', \omega)]$ where $\Delta\theta \equiv \theta_1 - \theta_2$ and

$$\theta' \equiv (1 - 2\epsilon)\Delta\theta, \beta' \equiv \epsilon(1 - \epsilon)(\Delta\theta)^2/(\theta - \gamma), \omega \equiv (\beta_1 - \beta_2)/\Delta\theta. \quad (45)$$

Since $\theta_j > \gamma$, then $\beta' \geq 0$. For definiteness, we choose the PDF indexed by 1 to be located at a larger mean and be in magnitude larger than that indexed by 2, so that $\Delta\theta > 0$, $\epsilon \leq 0.5$ and $\theta' \geq 0$. An additional constraint imposed by physics is that $\beta_j > 0$. The exact form of ξ_n' for $n \in [3, 5]$ is calculable and the results show that ξ_5' is particularly complex, making the finding of a reverse mapping based on all ξ_n' for $n \in [3, 5]$ a formidable task. A further problem in reaching a quantitative agreement with the statistics from the discrete model is the fact that those statistics may not be entirely of the form of Eq. 40, in which case the ξ_n' values are only an approximation to the true departure from the single Γ -PDF. For this reason, a simplification is introduced by restricting the inverse mapping to $[\xi_n' \text{ for } n = [3, 4] \rightarrow (\theta', \beta')]$ and ω is further

considered an empirical parameter. Therefore, it is understood that the ultimate mapping is only approximate, with possible consequences on the accuracy of the model.

Cumbersome and tedious calculations show that the solution to the inverse mapping is obtained by solving a cubic algebraic equation for one of the variables, and the other is found from a simple linear algebraic relationship [33]. In choosing the root of the cubic equation, the criterion is that β' should be the smallest positive root, because it is the one yielding the smallest ϵ , representing the smallest departure from the single- Γ -PDF. For specific values of ω , the cubic equation has easily computed roots. A thorough study of the root and solution behavior for various values of ω allowed a classification of the solution in two types according to the sign of $\Lambda \equiv [-2\xi'_3/(\theta-\gamma) - (\beta+\theta-\gamma)(7\beta+3\theta+\gamma-\xi'_4/\xi'_3)]/(\beta+\theta-\gamma)^2$. Specifically,

$\Lambda < 0$	$\Lambda > 0$
larger β_2	smaller β_2
$\omega = -0.62 + k_f \Lambda$	$\omega = -0.38 + k_s \Lambda$
$-2 \leq \omega \leq -0.62$	$-0.38 \leq \omega \leq w \frac{\beta}{\theta-\gamma}$
$k_f > 0$	$k_s > 0$ and $0 \leq w < 1$

and optimal values used in the calculations presented in the Results section are $k_f = 0.4$, $k_s = 0.8$ and $w = 0.67$. The condition $\Lambda \simeq 0$ is avoided, as it may lead to an irregular behavior.

Once θ' and β' are found, the other parameters of P_l are calculated as follows

$$\Delta\theta = \sqrt{(\theta')^2 + 4(\theta - \gamma)\beta'}, \quad \epsilon = 0.5(1 - \theta'/\Delta\theta) \quad (46)$$

$$\theta_1 = \theta + \epsilon\Delta\theta, \quad \theta_2 = \theta - (1 - \epsilon)\Delta\theta \quad (47)$$

$$\beta_1 = \beta - (1 + \omega)\beta' + \omega\epsilon\Delta\theta, \quad (48)$$

$$\beta_2 = \beta - (1 + \omega)\beta' - \omega(1 - \epsilon)\Delta\theta. \quad (49)$$

There are therefore 6 primary variables in the problem: D, T_d, ξ_{il} for $i \in [1, 4]$ and $N + 6$ secondary variables $q_i^{(s)}, j_{ji}^{(s)}, \theta_{1l}, \beta_{1l}, \theta_{2l}, \beta_{2l}$ and ϵ . Comparing with the discrete problem where there are $N + 2$ primary variables, it is immediately apparent that there is an advantage in adopting this formulations if $N > 4$.

Results

The discrete, single- Γ -PDF and double- Γ -PDF models were exercised for diesel fuel at the same initial and boundary conditions. The ordinary differential equations were solved using a fourth-order Runge-Kutta scheme with variable time step. The statistics extracted from the discrete model served as a reference, representing the desired behavior of the statistical or mixed models.

General considerations

Thermophysical properties

The evaporation rate and the drop temperature evolutions are strongly dependent on the thermophysical properties

of both liquid and gas phase. Generally, empirical or semi-empirical correlations used for the thermophysical properties are functions of m_i , or of m_i and T . For each thermophysical property, the same correlation is used for all models. All the correlations are presented in Appendix 1.

Number of components in the discrete model

Commercial fuels are composed of hundreds of species. Whereas in principle a discrete distribution model can reproduce a fuel with species belonging to many chemical families of hydrocarbons, for comparing results with those from CT-based models, we restrict our study to homologous families and specifically to paraffins. The lowest molar mass is specified according to the type of fuel, and for paraffins, the molar weight difference between adjacent species is 14 kg/kmole. Figure 1a shows such a discrete distribution with 32 paraffin species, where only 18 of the species are 'visible' on this scale (a logarithmic PDF scale starting at 10^{-12} still shows only 23 of the 32 species in the initial distribution). This 32-species distribution was used to create the database of discrete-model results that served as basis for comparison with the other models.

Inadequacy of the single- Γ -PDF model

Results from two calculations illustrate the problems of the single- Γ -PDF model. As a preliminary, consider a drop having an initial diameter $D_0 = 1$ mm at an initial temperature $T_{d,0} = 300$ K immersed in surroundings characterized by $T_g^{(\infty)} = 1000$ K and $Y_v^{(\infty)} = 0$, as in Run 1 listed on Table 1. Results depicted in Fig. 2 show comparisons between the discrete and the single- Γ -PDF models. Both models predict the same variation of D^2/D_0^2 and T_d , and $X_v^{(s)}$ differs only in the last stages of evaporation (see Fig. 2a). In contrast to the traditional single-component drop evaporation where T_d reaches a steady state, here T_d continues to increase owing to the linear dependency of the boiling temperature on the mean molar weight. One major difference between the discrete and single- Γ -PDF models is in the evolution of the liquid composition, shown in Fig. 2b. Whereas there is reasonable agreement between the θ_l values, there are large quantitative discrepancies between the predicted σ_l values, although both models predict a reduction in σ_l . These discrepancies start early in the drop lifetime and cannot be ignored. The evolutions of the liquid discrete-model PDF and the single- Γ -PDF are illustrated in Fig. 2c at several stages of the drop lifetime. The PDF from the discrete model is plotted as the envelope of the bar chart that represents the discrete model results. The gradual departure of the single- Γ -PDF from the discrete-model PDF is easily observable. Finally, the impact of these discrepancies on the surface vapor composition is displayed in Fig. 2d where it is evident that the single- Γ -PDF surface vapor standard deviation is smaller by 10% than that predicted by the discrete model.

In sprays, drops evaporate in an environment that already contains vapor. During MC-fuel drop evaporation

there is therefore a complete coupling between the evolution of the species from the drop and both the far-field vapor mass fraction and the far-field vapor composition. To understand the behavior of the single- Γ -PDF under these circumstances, consider the conditions of Run 2 listed in Table 1. For Run 2, all initial conditions are the same as in Run 1, except that $Y_v^{(\infty)} = 0.82$ with the composition of the far field vapor specified as shown in Table 1. Plots equivalent to those of Fig. 2 are presented in Fig. 3. The presence of a relatively large amount of vapor in the gas phase induces initial drop net condensation and the drop grows in size, as shown in Fig. 3a. After this initial transient, net evaporation begins during which, following a short transient, the linear D^2 -law is recovered. Initially, T_d increases more sharply than in Fig. 2a because the condensed mass adds heat to the drop in the form of latent heat. Similar to the comparison in Fig. 2, there is excellent agreement between the discrete and the single- Γ -PDF model predictions for D^2/D_0^2 and T_d , and $X_v^{(s)}$ differs only after the drop residual mass is less than 15%. Examination of Fig. 3b reveals that the initial condensation results in a decrease in θ_l and a concomitant increase in σ_l which accounts for the species added to the liquid mixture. Further evaporation results in an increase in θ_l and a decrease in σ_l , as shown by the results from the discrete model. However, the single- Γ -PDF results display the opposite behavior in σ_l in that it increases. Thus, unlike when $Y_v^{(\infty)} = 0$, now it is no longer only the quantitative values but the qualitative trends that are not captured by the single- Γ -PDF model. This fact is easily observable in Fig. 3c where the discrete model distribution displays another, smaller peak as evaporation proceeds, which the single- Γ -PDF model inherently cannot replicate. It is the emergence of this second peak that prompted the development of a new model based on the superposition of two Γ -PDFs. Fig. 3d shows the discrepancies between the discrete and single- Γ -PDF model predictions for the vapor composition.

One noteworthy result of these comparisons is that neither one of D^2/D_0^2 , T_d , or $X_v^{(s)}$ evolutions is a good indicator that a model captures the composition aspects of the liquid or the gas. This observation has important implications in that experimental results focussing on these three variables are not adequate to validate models. It is obvious that composition measurements are necessary to determine whether a model is appropriate.

Results from the double- Γ -PDF model

All initial and boundary conditions of the computations are listed in Table 1. Emulating Lippert (1999), in most test cases the far-field vapor composition is chosen to be the initial equilibrium vapor composition at the drop surface; this is indeed the most likely environment encountered by a newly injected drop as it represents the most volatile components that would have evaporated from already injected drops. The double- Γ -PDF model evaluation is performed prior to focussing on the study of the

influence of $T_g^{(\infty)}$ (Runs 2-4), then on that of $X_v^{(\infty)}$ (Runs 2, 5 and 6), further on the far field composition (Runs 2, 7 and 8), and finally on the transport coefficients effects through the value of the Le (Runs 2, 9 and 10). As stated above, T_d , D^2/D_0^2 and $X_v^{(s)}$ predictions are insensitive to the fuel composition, and thus in the following illustrations they will be presented for the discrete model only.

Parametric study

Temperature variation In Fig. 4a are illustrated T_d and D^2/D_0^2 for $T_g^{(\infty)} = 600, 1000$ and 1200 K (Runs 4, 2 and 3). In all cases the drop initially experiences net condensation before net evaporation begins. Although the extent of net condensation evident from the drop growth decreases with increasing $T_g^{(\infty)}$, the initial drop growth rate seems independent of $T_g^{(\infty)}$. The rate of heat transfer to the drop increases with $T_g^{(\infty)}$, and T_d and $X_v^{(s)}$ (see Fig. 4b) become larger earlier. During the initial net condensation $X_v^{(s)}$ becomes eventually larger than $X_v^{(\infty)}$ but a slight decline occurs during net evaporation. Comparisons between the discrete model and double- Γ -PDF predictions are presented in Figs. 4c through 4f for θ_l , σ_l , $\theta_v^{(s)}$ and $\sigma_v^{(s)}$. The agreement between the two models is very good to excellent. Particularly, $\theta_v^{(s)}$ and $\sigma_v^{(s)}$, which are the quantities of interest in predicting the composition of the gas phase are very accurately predicted. During net condensation, σ_l increases and θ_l decreases due to the addition of the lighter, far-field species; as net evaporation initiates, the lighter species leave the drop, resulting in the reverse trend.

Finally, Figs. 4g and 4h portray a comparison between the discrete model and the double- Γ -PDF of the surface vapor at two times corresponding to a residual liquid mass of 60% and 20% respectively. At the smallest $T_g^{(\infty)}$ and early in the drop lifetime, the PDF visibly has a single peak which is located in the lower- m regime of the double- Γ -PDF, consistent with the fact that during slow drop heating the more volatile components are first released from the drop. Another, minor peak which was barely evident during the early drop lifetime develops in the larger- m regime during the later stages of the drop life. For the larger values of $T_g^{(\infty)}$ and at 60% of residual liquid mass, the lower- m regime peak is the minor of the two peaks, but becomes dominant later during the drop lifetime. The physical explanation for this behavior is that at higher ambient temperature, the less volatile components may also evaporate because there is a larger heat flux into the drop leading to a higher drop temperature. Comparing the size of the two peaks, the longest net condensation period which occurs at the smallest $T_g^{(\infty)}$ naturally leads to the largest peak at the lower- m regime of the double- Γ -PDF. The double- Γ -PDF faithfully captures the discrete model both in the early and later stage of the drop lifetime and thus reproduces the differential species evaporation as a function of $T_g^{(\infty)}$. The importance of the domi-

nant lighter components in the gas composition highlights the necessity of the double- Γ -PDF representation.

To understand the relationship between the lower m peak in the surface vapor and liquid PDFs, consider the PDF of the liquid composition illustrated in Fig. 5 at the two times corresponding to a residual liquid mass of 60% (Fig. 5a) and 20% (Fig. 5b). At 60% of the residual mass, the PDFs display generally a single peak, although a nascent lower- m protuberance is emerging. At 20% of the residual mass, the lower- m regime peak is evident in all PDFs and its magnitude increases with decreasing $T_g^{(\infty)}$, that is with increasing initial net condensation period which lead to the largest peak in the lower- m regime for the surface vapor composition PDF. This difference between the lowest $T_g^{(\infty)}$ PDF and those at larger $T_g^{(\infty)}$ is consistent with the σ_l behavior and excellently captured by the double- Γ -PDF at all stages of the drop lifetime. Thus, although the surface vapor composition is eventually dominated by the low molar weight species, the liquid composition still peaks at a relatively large molar weight during the earlier part of the drop lifetime and is dominated by the higher components during the later part of the drop lifetime. The fact that relatively light components remain inside the drop close to the end of the drop life is noticeable and is the result of eventual saturation. The double- Γ -PDF representation faithfully replicates the discrete model.

Since the evolution from the initial condition, single- Γ -PDF to the double- Γ -PDF is represented in Eq. 40 by the magnitude of ϵ , in Fig. 5c we depict its time variation. At the lowest $T_g^{(\infty)}$, ϵ displays a sharp increase from its initial null value, then decreases and after a ‘kink’, it evolves with a continuing non-monotonic behavior. The same general behavior, but with less dramatic variations is exhibited at the two other $T_g^{(\infty)}$ values, and ϵ decreases with increasing $T_g^{(\infty)}$. Although ϵ is small with respect to unity (here $\epsilon \in [0.02, 0.27]$), it specifically allows the development of the minor, lower- m peak in the liquid PDF which translates into the dominant, lower- m in the surface vapor PDF.

Effect of the far-field mole fraction To explore the effect of $X_v^{(\infty)}$, we compared results from Runs 2, 5 and 6. The net condensation rate in the early stages of the drop lifetime increases with $X_v^{(\infty)}$ as shown in Fig. 6a, leading to larger drops before net evaporation begins. Consistent with the higher net condensation rate, the initial dT_d/dt is larger as well. Initially, $X_v^{(s)}$ increases during the net condensation period, but an eventual asymptotic behavior develops (see Fig. 6b). The agreement of the double- Γ -PDF with the discrete model is excellent for θ_l , $\theta_v^{(s)}$ and $\sigma_v^{(s)}$, and very good to fair for σ_l , as illustrated in Figs. 6c to 6f. The small glitch in the $\theta_v^{(s)}$ and $\sigma_v^{(s)}$ curves for $X_v^{(\infty)} = 0.1$ corresponds to the time when ϵ experiences a sharp change in curvature (e.g. Fig. 5c) but the model is robust enough to overcome this small, local timewise discontinuity and

the computation quickly recovers and continues to lead to excellent agreement with the discrete model. We note that the excellent agreement on $\theta_v^{(s)}$ and $\sigma_v^{(s)}$ is a key element for robust two-phase flow computations.

Comparison of the surface vapor double- Γ -PDF with the discrete model PDF at 60% and 20% of the initial mass is presented in Figs. 6g and 6h. At 60% residual mass, a minor peak in the discrete distribution is already visible which is fairly well replicated by the double- Γ -PDF. By 20% residual mass, the minor peak at 60% residual mass becomes dominant and all double- Γ -PDFs reproduce the result of the discrete model with remarkable accuracy. The second peak increases with $X_v^{(\infty)}$, which together with the fact that it also increased with decreasing $T_g^{(\infty)}$ suggests that it is due to the condensation process. Such condensation is inevitable in sprays where drops are transported in regions of different temperature and composition, and the capturing of this physics is considered essential to the model utilization under spray conditions.

Comparison of the respective effects of $T_g^{(\infty)}$ and $X_v^{(\infty)}$ shows that the former has a much larger impact on the vapor composition. In fact, $\sigma_v^{(s)}$ is almost independent of $X_v^{(\infty)}$.

Effect of the ambient composition In Fig. 7 we compare results from Runs 2, 7 and 8 in order to assess the influence of $\theta_v^{(\infty)}$ and $\sigma_v^{(\infty)}$ on the predictions. Apparently, neither T_d or D^2/D_0^2 (Fig. 7a) nor $X_v^{(s)}$ (Fig. 7b) are sensitive to the far field composition. What matters for the magnitude of these variables is the far-field vapor molar fraction but not the vapor composition. This explains why these parameters are insensitive to the model used (single- Γ -PDF versus double- Γ -PDF). The drop net growth rate is the same for all three runs and only a small increase in D^2/D_0^2 and in the duration of condensation is discernible with increasing $\theta_v^{(\infty)}$ and $\sigma_v^{(\infty)}$. As for θ_l , $\theta_v^{(s)}$ and $\sigma_v^{(s)}$, the agreement of the double- Γ -PDF with the discrete model is excellent (Figs. 7c, 7e and 7f), while σ_l (Fig. 7d) is very well predicted during most of the drop lifetime. While it would be desirable to have a better replication of σ_l by the double- Γ -PDF, we reiterate that in fact it is the prediction of $\theta_v^{(s)}$ and $\sigma_v^{(s)}$ that is important in spray calculations for which this model is being developed.

The suggestion that the lower- m peak in the double- Γ -PDF originates from condensation is strengthened by the plots of the surface vapor PDF at 60% (Fig. 7g) and 20% (Fig. 7h) residual mass. At 60% residual mass, all PDF exhibit two peaks and for the smallest $\theta_v^{(\infty)}$ the magnitude of the lower- m peak is already dominant. During the entire drop evolution, the magnitude of the lower- m peak depends inversely on the initial liquid-PDF mean. Further adding to the argument that the condensation process is responsible for the minor peak is the fact that the molar weight composition of that peak is similar to that of the far field. The agreement of the double- Γ -PDF with the discrete model is very good.

Since all results seem to indicate that the minor peak results from the condensation process, it is of interest to follow the history of the liquid mass fraction associated with specific molar weights. Plots of these quantities computed from the discrete model for two different far-field conditions are illustrated in Fig. 8. In a vapor-free environment such as in Run 1 (Fig. 8a), the mass fractions monotonically decrease and the lighter components disappear earlier from the drop. In an environment with vapor in the far field, such as in Run 2 (Fig. 8b), there are species of molar weight much larger than $\theta_v^{(\infty)}$ whose liquid mass fraction decreases monotonically, and species of molar weight comparable to $\theta_v^{(\infty)}$ whose liquid mass fraction initially increases, which corresponds to condensation, reach a peak, and then decrease, which corresponds to evaporation. The purpose of this examination is to underline the fate of different species according to how their molar weight compares to the composition of the far field, and also to highlight the fact that the drop evolution is the combined manifestation of these different histories. This is precisely where lies the difficulty in developing an appropriate representation of MC-fuel drop evaporation using as few equations as possible.

Gas Lewis number variation Lewis number effects (Runs 2, 9 and 10) are illustrated in Fig. 9. As Le increases, the characteristic time for mass diffusion becomes larger with respect to that of heat diffusion in the gas phase. This means that condensation is delayed with increasing Le , which in turn leads to a lower rate of T_d increase (Fig. 9a) corresponding to the smaller and delayed drop growth (Fig. 9a) and to a delayed achievement of the steady-state evaporation. Thus, drops in a gas having a smaller Le grow faster and to larger size as the initial net condensation is more effective, and they evaporate slightly faster. The much larger rate of increase in $X_v^{(s)}$ for the smallest Le (Fig. 9b) portrays the faster condensation, and the earlier reaching of an asymptotic behavior is consistent with an earlier steady state. The steady-state value of $X_v^{(s)}$ is larger with increasing Le because the increased mass diffusion time means that the evaporated species tend to stay longer at the surface.

This physical picture is confirmed by Figs. 9d - 9f. We note that for all θ_l , $\theta_v^{(s)}$ and $\sigma_v^{(s)}$ the double- Γ -PDF results are in excellent agreement with those of the discrete model, and for σ_l the agreement is very good up to a residual mass of 9%, after which a deterioration is observed at the lower Le . θ_l varies inversely with Le but $\theta_v^{(s)}$ decreases with decreasing Le , although the relative variation of θ_l and $\theta_v^{(s)}$ is considerably smaller than that in Le , showing that the prediction of this quantity is relatively insensitive to the uncertainties associated with the exact knowledge of \mathcal{D}_{eff} . Both σ_l and $\sigma_v^{(s)}$ are decreasing functions of Le , showing that liquid mixtures have fewer species with increasing Le .

Examination of the surface vapor PDFs at 60% residual mass (Fig. 9g) shows in all cases the initiation of a minor peak which is located at smaller m with increas-

ing Le . The distribution is wider with decreasing Le . By 20% residual mass (Fig. 9h), the lower- m peak has become dominant only for the smallest Le value, indicating the retention of the enhanced effect of the lower- m species seen earlier in the lifetime. The agreement of the double- Γ -PDF with the discrete model is very good for largest Le and excellent for the smallest Le .

Conclusions

A model has been developed to describe the evaporation of a drop of a multicomponent fuel containing a multitude of species. The model adopts a statistical representation through a distribution function, based on Continuous Thermodynamics concepts. Unlike a precedent model, the present model is not based on the distribution function retaining during drop evaporation its original mathematical form of a single Gamma Probability Distribution Function (single- Γ -PDF) specified as a function of the molar weight. This change in representation is in response to the observation that when the single- Γ -PDF is assumed to represent the fuel distribution during evaporation, it leads to strong departures from the results obtained with a discrete model accounting for all individual species in the mixture. The discrete model was exercised for 32 paraffin species making it numerically tractable, allowing the accounting of species of interest in petroleum fuels, and enabling the extraction of statistics that serve as the baseline results against which all other models are compared. Such a set of baseline results is necessary as it is also shown that quantities usually measured to describe drop evaporation, such as residual drop surface area, drop temperature or vapor mass fraction at the drop surface are insensitive to the drop and surrounding gas composition.

The new model describing drop evaporation is based on the evolution of the single- Γ -PDF representing the initial liquid fuel composition to a superposition of two Γ -PDFs, a form which is called the double- Γ -PDF. This form is suggested by results from the discrete model which show that when a drop is immersed into gaseous surroundings whose composition includes light species (as would be the case in sprays used in energy producing devices, because of the light species already evaporated from other drops), condensation of these light species creates a minor peak of the distribution at the lower end of the molar weight. To replicate this behavior, one must determine the double- Γ -PDF by computing its five parameters: two for each of the two Γ -PDFs and the height of the minor peak. This problem of determining the five parameters is reduced to an inverse mapping of the distribution first five moments to the five parameters of the double- Γ -PDF. This inverse mapping is accomplished only approximately using the first four moments and a parameter whose value is empirically determined; this is, however, not considered crucial to the final results because the discrete model PDF may actually not be entirely in double- Γ -PDF form.

Extensive comparisons of the double- Γ -PDF with the statistics from the discrete representation for diesel fuel

show that the predictions of the model can be qualified as excellent for the composition of the vapor fuel at the drop surface which determines the vapor composition. Excellent predictions are also obtained for the mean molar weight of the liquid, however, the predictions of the liquid molar weight standard deviation is excellent to fair, depending on the situation. It is also shown that the accuracy of the predictions depends to a great extent on the double- Γ -PDF being able to capture the liquid-distribution minor peak that evolves as a result of condensation. This peak is minor for the liquid composition, however, for the vapor it may be of similar magnitude as the high-molar-weight peak during the early drop lifetime and even dominate the drop-surface vapor composition in the later stage of the drop lifetime.

Appendix 1: Correlations of thermophysical properties

In the calculations, air is treated as a single pseudo-component, inert carrier gas with an effective critical temperature $T_c = 133$ K, molar weight $m_a = 29$ g/mole and ratio of heat capacities $\gamma_a = 1.4$. Then, $\lambda_a = 1.36 \times 10^{-2}(T/T_c)^{0.75}$ (W/mK) and $C_p = \gamma_a R_u / (\gamma_a - 1) m_a$ (J/gK) where $R_u = 8.3142$ (J/moleK) where the subscript c denotes the critical point.

We adopted Trouton's rule which states that $m_i L_{vi} / (R_u T_{bi}) = 10.6$, and used information from [34] to obtain the correlation $T_b(m_i) = 241.4 + 1.45 m_i$ (K). Information from [34] also allowed the development of the following correlation

$$\lambda_v(m_i) = 3.45 \times 10^{-3} m_i^{0.37} \left(\frac{T}{T_b} \right)^n \text{ (W/mK).}$$

where $n = 2.225 m_i / (m_i + 19.245)$. The correlations for the heat capacities were those of [15], namely $C_p(m_i) = (A_p + B_p m_i) R_u / m_i$ (J/gK) where $A_p = 2.465 - 0.1144 T + 1.759 \times 10^{-5} T^2 - 5.972 \times 10^{-9} T^3$, $B_p = -0.3561 + 9.367 \times 10^{-4} T - 6.030 \times 10^{-7} T^2 + 1.324 \times 10^{-10} T^3$. For both $\lambda_v(m_i)$ and $C_p(m_i)$, the calculation is made at the surface conditions, that is T_d and $m_v^{(s)}$. Also following [15], $C_l = 2.26 - 2.94 \times 10^{-3} T_d + 9.46 \times 10^{-6} T_d^2$ (J/gK). To calculate properties for a mixture, we used mixing rules based on mass fractions.

ACKNOWLEDGMENTS

This research was performed at the Jet Propulsion Laboratory (JPL) of the California Institute of Technology, under the partial sponsorship of U.S. Department of Energy (DOE), with Mr. Neil Rossmeyssl and Ms. Roxanne Danz (DOE Headquarters), and Mr. D. Hooker (DOE Golden Center) serving as contract monitors, under an agreement with the National Aeronautics and Space Administration. Additional sponsorship was provided by the Donors of The Petroleum Research Fund administered by the American Chemical Society through a grant to one of the authors (JB) that supported a Caltech Post Doctoral Fellow (PCLeC).

References

- [1] Law, C. K., Prakash, S. and Sirignano, W. A. 1976. Theory of convective, transient, multicomponent droplet vaporization, *Proc. Comb. Inst.*, 16, 605-617
- [2] Lara-Urbaneja, P. and Sirignano, W. A. 1981. Theory of transient multicomponent droplet vaporization in a convective field, *Proc. Comb. Inst.*, 18, 1365-1374
- [3] Harstad, K. and J. Bellan, J. 1991. A model of the evaporation of binary-fuel clusters of drops, *Atomization and Sprays*, 1, 367-388
- [4] Law, C. K. and Law, H. K. 1982. A d^2 - law for multicomponent droplet vaporization and combustion, *AIAA J.*, 20(4), 522-527.
- [5] Hanson, S. P., Beer, J. M. and Sarofim, A. F. 1982. Non-equilibrium effects in the vaporization of multicomponent fuel droplets, *Proc. Comb. Inst.*, 19, 1029-1036
- [6] Sorbo, N. W., Law, C. K., Chang, P. Y. and Steeper, R. R. 1989. An experimental investigation of the incineration and incinerability of chlorinated alkane drops, *Proc. Comb. Inst.*, 22, 2019-2026
- [7] Randolph, A. L., Makino, A. and Law, C. K. 1986. Liquid-phase diffusional resistance in multicomponent droplet gasification, *Proc. Comb. Inst.*, 21, 601-608
- [8] Wang, C. H., Liu, X. Q. and Law, C. K. 1984. Combustion and microexplosion of freely falling multicomponent droplets, *Combust. Flame*, 56(2), 175-197
- [9] Yang, J. C. and Avedesian, C. T., 1988. The combustion of unsupported heptane/hexadecane mixture droplets at low gravity, *Proc. Comb. Inst.*, 22, 2037-2044
- [10] Jackson, G. S., Avedesian, C. T. and Yang, J. C. 1992. Observations of soot during droplet combustion at low gravity - heptane and heptane monochloroalkane mixtures, *Int. J. Heat Mass Transfer*, 35(8), 2017-2033
- [11] Gökalp, I., Chauveau, C., Berrekam, H. and Ramos-Arroyo, N. A. 1994. Vaporization of miscible binary fuel droplets under laminar and turbulent convective conditions, *Atomization and Sprays*, 4, 661-676
- [12] Marchese, A. J., Dryer, F. L., Colantonio, R. O. and Nayagam, V. 1996. Microgravity combustion of methanol and methanol/water droplets: drop tower experiments and model predictions, *Proc. Comb. Inst.*, 26, 1209-1217
- [13] Wood, B. J., Wise, H. and Inami, S. H. 1960. Heterogeneous combustion of multicomponent fuels, *Combust. Flame*, 4(3), 235-242
- [14] Wong, S. C. and Lin, A. C. 1992. Internal temperature distributions of droplets vaporizing in high-temperature convective flows, *J. Fluid Mech.*, 237, 671-687

- [15] Tamim J. and Hallett W. L. H. 1995. A continuous thermodynamics model for multicomponent droplet vaporization, *Chem. Eng. Sci.*, 50(18), 2933-2942.
- [16] Hallett W. L. H. 2000. A simple model for the vaporization of droplets with large numbers of components, *Combust. Flame*, 121,334-344
- [17] Lippert A. M. 1999. Modeling of multicomponent fuels with application to sprays and simulation of Diesel engine cold start, Ph. D. Thesis, University of Wisconsin, Madison.
- [18] Lippert, A. M. and Reitz, R. D. 1997. Modeling of multicomponent fuels using continuous distributions with application to droplet evaporation and sprays, SAE Paper 972882
- [19] Bowman, J. R. and Edmister, W. C., 1951 Flash distillation of an indefinite number of components, *Ind. Chem. Eng.*, 43, 2625-2628
- [20] Edmister, W. C. and Bowman, J. R. 1952. Equilibrium conditions of flash vaporization of petroleum fractions, *Chem. Eng. Prog. Symp. Ser.*, 48, 46-51
- [21] Aris R. and Gavalas G. R. 1966. On the theory of reactions in continuous mixtures, *Phil. Trans. R. Soc. A* 260, 351-393.
- [22] Briano, J. G. and Glandt, E. D 1983.. Molecular thermodynamics of continuous mixtures, *Fluid Phase Equilibria*, 14, 91-102
- [23] Cotterman, R. L., Bender, R. and Prausnitz, J. M. 1985. Phase equilibria for mixtures containing very many components. Development and application of continuous thermodynamics for chemical process design, *Ind. Eng. Chem. Process Des. Dev.*, 24, 194-203
- [24] Gal-Or, B., Cullinan, Jr., H. T. and Galli, R. 1975. New thermodynamic-transport theory for systems with continuous component density distributions, *Chem. Eng. Sci.*, 30, 1085-1092
- [25] Harstad, K. and J. Bellan, J., 2000. An All-Pressure Fluid Drop Model Applied to a Binary Mixture: Heptane in Nitrogen, *Int. J. of Multiphase Flow*, 26(10), 1675-1706
- [26] Keizer, J. 1987 *Statistical thermodynamics of nonequilibrium processes*, Springer-Verlag, New York
- [27] Hirshfelder, J. O., Curtis, C. F. and Bird, R. B. 1954. *Molecular Theory of Gases and Liquids*, John Wiley and Sons, Inc.
- [28] Giovangigli, V. 1991 Convergent Iterative Methods for Multicomponent Diffusion, *IMPACT Comput. Sci. Eng.*, 244-276
- [29] Giovangigli, V. 1999 *Multicomponent Flow Modeling*, Birkhäuser, Boston, MESST Series
- [30] Williams, F. A. 1965. *Combustion Theory*, Addison-Wesley
- [31] LeClercq, P. C. and Bellan, J., 2002 Direct numerical simulation of a transitional temporal mixing layer laden with multicomponent-fuel evaporating drops using continuous thermodynamics, submitted to *J. Fluid Mech.*
- [32] Whitson C. H. 1983. Characterizing hydrocarbon plus fractions, *Soc. Pet. Eng. J.*, 23, 683-694.
- [33] Harstad, K.G, Le Clercq, P. C. and J. Bellan, J., 2002 A statistical model of multicomponent-fuel drop evaporation for many-drop gas-liquid flow simulations, submitted to the *Int. J. Multiphase Flow*
- [34] American Petroleum Institute, 1992. *Technical Data Book - Petroleum Refining*, American Petroleum Institute, Fifth Edition

Run	$X_v^{(\infty)}(Y_v^{(\infty)})$	$\theta_v^{(\infty)}$	$\sigma_v^{(\infty)}$	Le	$T_g^{(\infty)}$ (K)
1	0	-	-	0.5	1000
2	0.5(0.82)	131.3	24.4	0.5	1000
3	0.5(0.82)	131.3	24.4	0.5	1200
4	0.5(0.82)	131.3	24.4	0.5	600
5	0.3(0.66)	131.3	24.4	0.5	1000
6	0.1(0.33)	131.3	24.4	0.5	1000
7	0.5(0.82)	120	18	0.5	1000
8	0.5(0.82)	140	28	0.5	1000
9	0.5(0.82)	131.3	24.4	1	1000
10	0.5(0.82)	131.3	24.4	2	1000

Table 1: For all simulations $\theta_l = 185$ kg/kmole, $\sigma_l = 43$ kg/kmole and $\gamma_l = 86$ kg/kmole. The units for $\theta_v^{(\infty)}$ are kg/kmole. In all runs $D_0 = 1$ mm and $T_{d,0} = 300$ K.

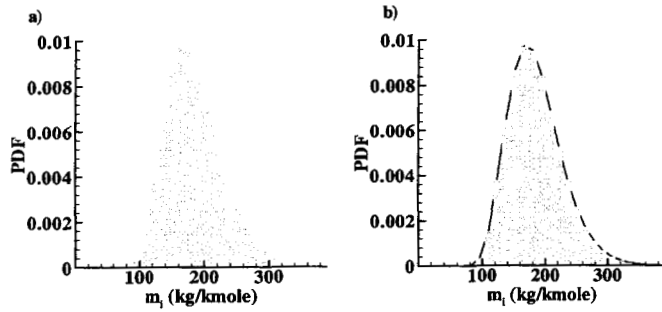


Figure 1: Probability Density Functions (PDFs) used in the computations. (a) Discrete pseudo-components $\gamma = 86$ kg/kmole, $\theta_{l,0} = 185$ kg/kmole, $\sigma_{l,0} = 43$ Only 18 out of the 32 components are ‘visible’ on this scale. (b) The single- Γ -PDF envelope of the initial discrete PDF.

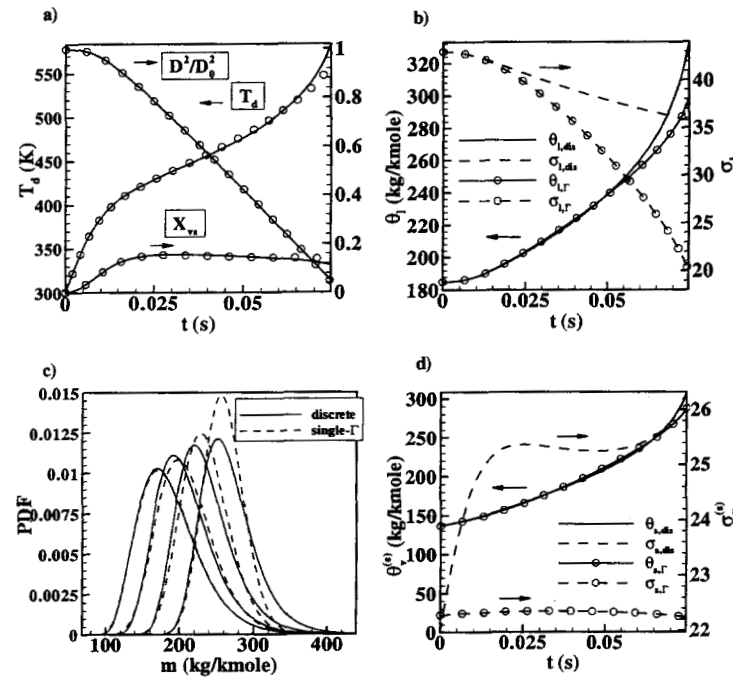


Figure 2: Evaporation of a diesel fuel drop in a vapor-free environment (Run 1 of Table 1), discrete model vs the single- Γ -PDF model. a) Drop temperature, relative surface area and surface vapor mole fraction evolution in time; lines for the discrete model and symbols for the single- Γ -PDF, b) Liquid mean molar weight and standard deviation evolution in time, c) PDF at different stages of evaporation; from left to right 90%, 60%, 30% and 10% remaining mass, d) Surface mean molar weight and standard deviation evolution in time.

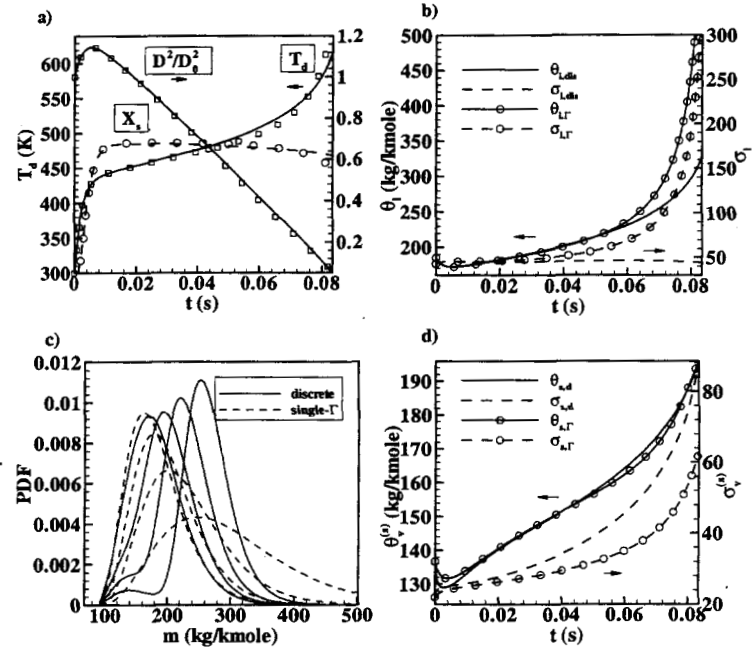


Figure 3: Evaporation of a diesel fuel drop, discrete model vs the single- Γ -PDF model (Run 2 of Table 1). a) Drop temperature, relative surface area and drop surface vapor mole fraction; lines for discrete model, symbols for the single- Γ -PDF. b) liquid mean molar weight and standard deviation evolution in time, c) PDF at different stages of evaporation; from left to right 90%, 60%, 30% and 10% remaining mass, d) Surface mean molar weight and standard deviation evolution in time.

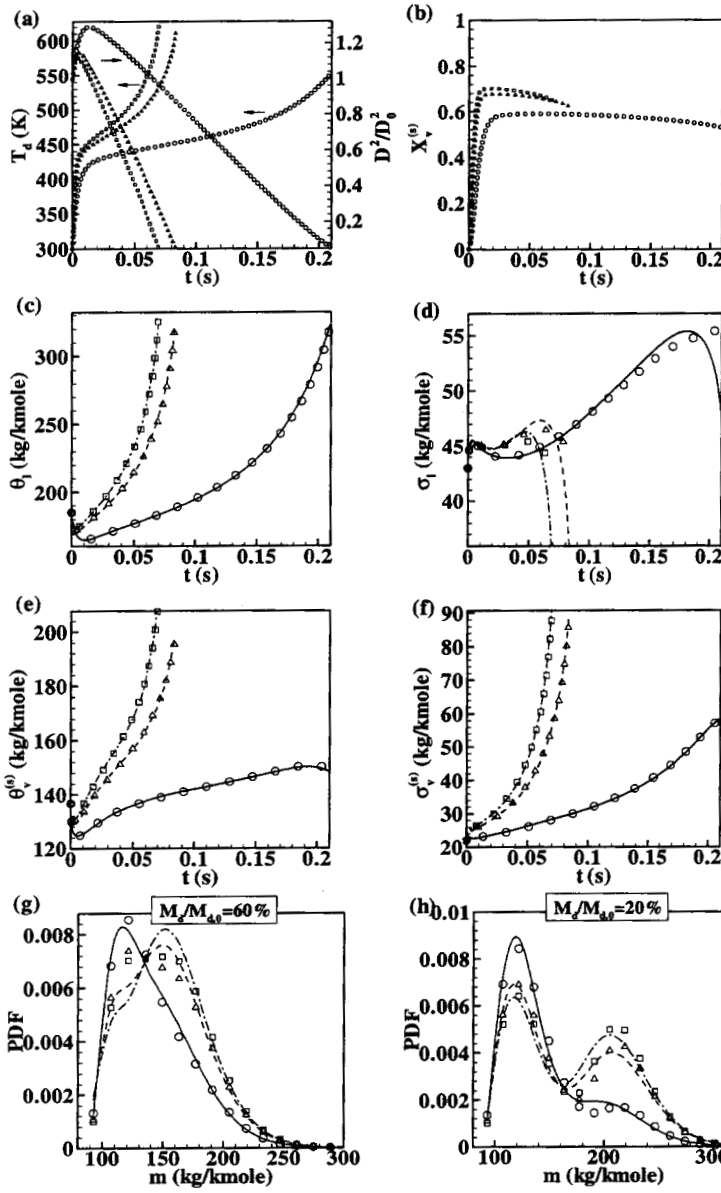


Figure 4: Drop history for Runs 2 - 4 of Table 1: — and \circ for $T_g^{(\infty)} = 600K$, - - - and Δ for $T_g^{(\infty)} = 1000K$ and - · - and \square for $T_g^{(\infty)} = 1200K$. Discrete (symbols) versus double- Γ -PDF (lines) model. (a) Drop temperature and relative surface area (discrete model only), (b) Drop surface vapor mole fraction (discrete model only), (c) Liquid mean molar weight, (d) Liquid PDF standard deviation, (e) Surface composition mean molar weight, (f) Surface composition PDF standard deviation, (g) Surface vapor PDFs at 60% residual drop mass, and (h) Surface vapor PDFs at 20% residual drop mass.

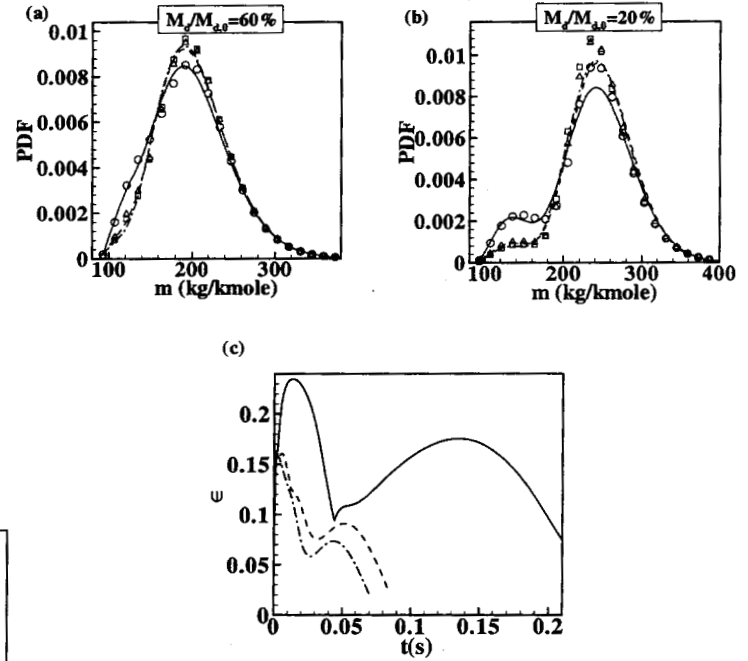


Figure 5: Characteristics of the liquid double- Γ -PDF for Runs 2 - 4 of Table 1. (a) PDF at 60% of the drop initial mass, (b) PDF at 20% of the drop initial mass and (c) ϵ timewise evolution.

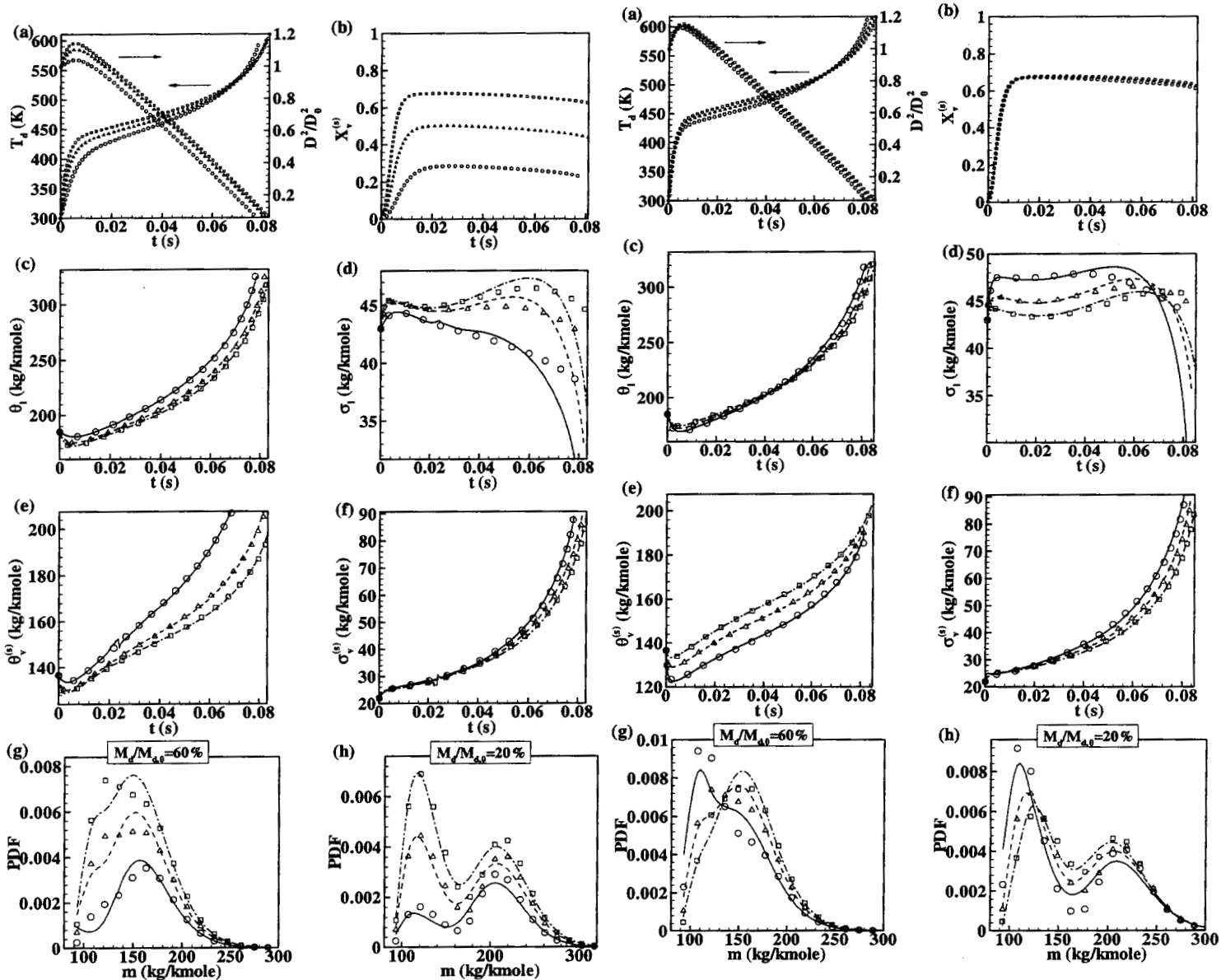


Figure 6: Drop history for Runs 2, 5 and 6 of Table 1: — and \circ for $X_v^{(\infty)} = 0.1$, - - - and Δ for $X_v^{(\infty)} = 0.3$ and - · - and \square for $X_v^{(\infty)} = 0.5$. Discrete (symbols) versus double- Γ -PDF (lines) model. (a) Drop temperature and relative surface area (discrete model only), (b) Drop surface vapor mole fraction (discrete model only), (c) Liquid mean molar weight. (d) Liquid PDF standard deviation, (e) Surface composition mean molar weight, (f) Surface composition PDF standard deviation, (g) Surface vapor PDFs at 60% residual drop mass, and (h) Surface vapor PDFs at 20% residual drop mass.

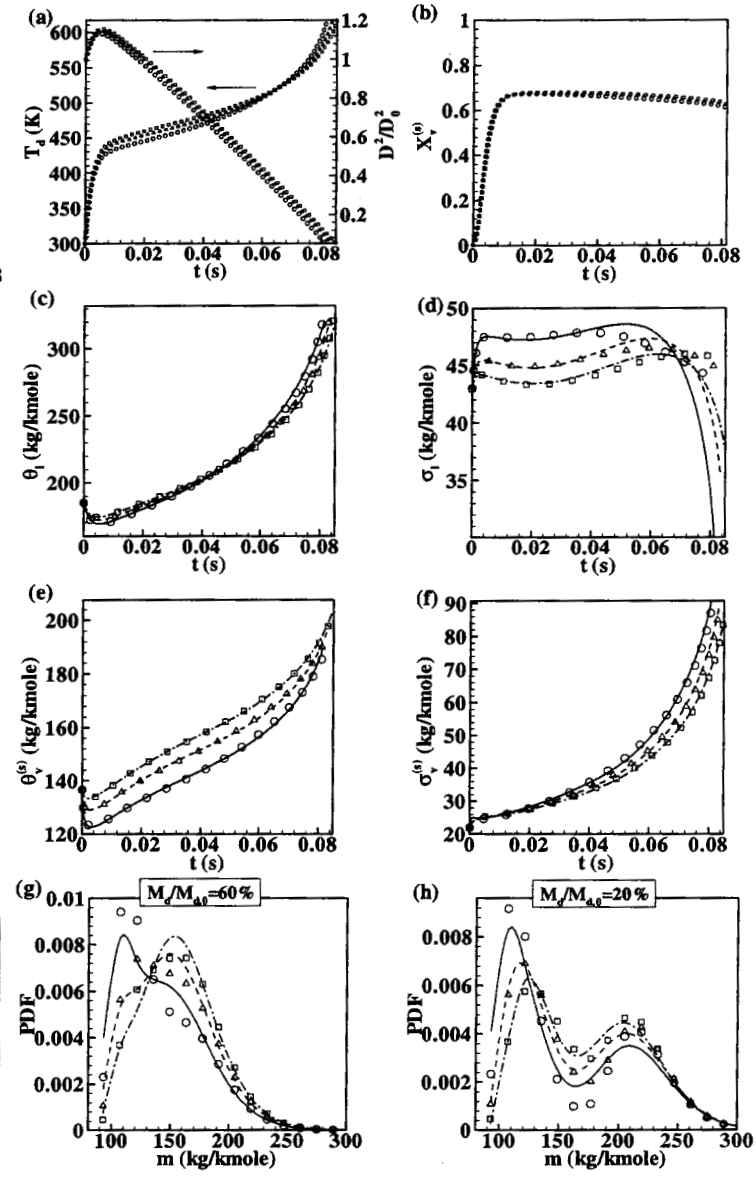


Figure 7: Drop history for Runs 2, 7 and 8 of Table 1: — and \circ for $\theta_v^{(\infty)} = 120$ kg/kmole, $\sigma_v^{(\infty)} = 18$, - - - and Δ for $\theta_v^{(\infty)} = 131.3$ kg/kmole, $\sigma_v^{(\infty)} = 24.4$ and - · - and \square for $\theta_v^{(\infty)} = 140$, $\sigma_v^{(\infty)} = 28$. Discrete (symbols) versus double- Γ -PDF (lines) model. (a) Drop temperature and relative surface area (discrete model only), (b) Drop surface vapor mole fraction (discrete model only), (c) Liquid mean molar weight, (d) Liquid PDF standard deviation, (e) Surface composition mean molar weight, (f) Surface composition PDF standard deviation, (g) surface vapor PDFs at 60% residual drop mass, and (h) Surface vapor PDFs at 20% residual drop mass.

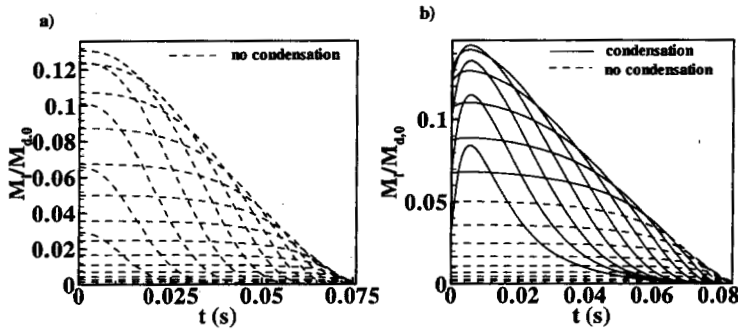


Figure 8: Timewise evolution of non-dimensionalized species partial mass for a) vapor-free environment (Run 1) and b) $X_v^{(\infty)} = 0.5$, $\theta_v^{(\infty)} = 131.3$ kg/kmole, $\sigma_v^{(\infty)} = 24.4$ (Run 2).

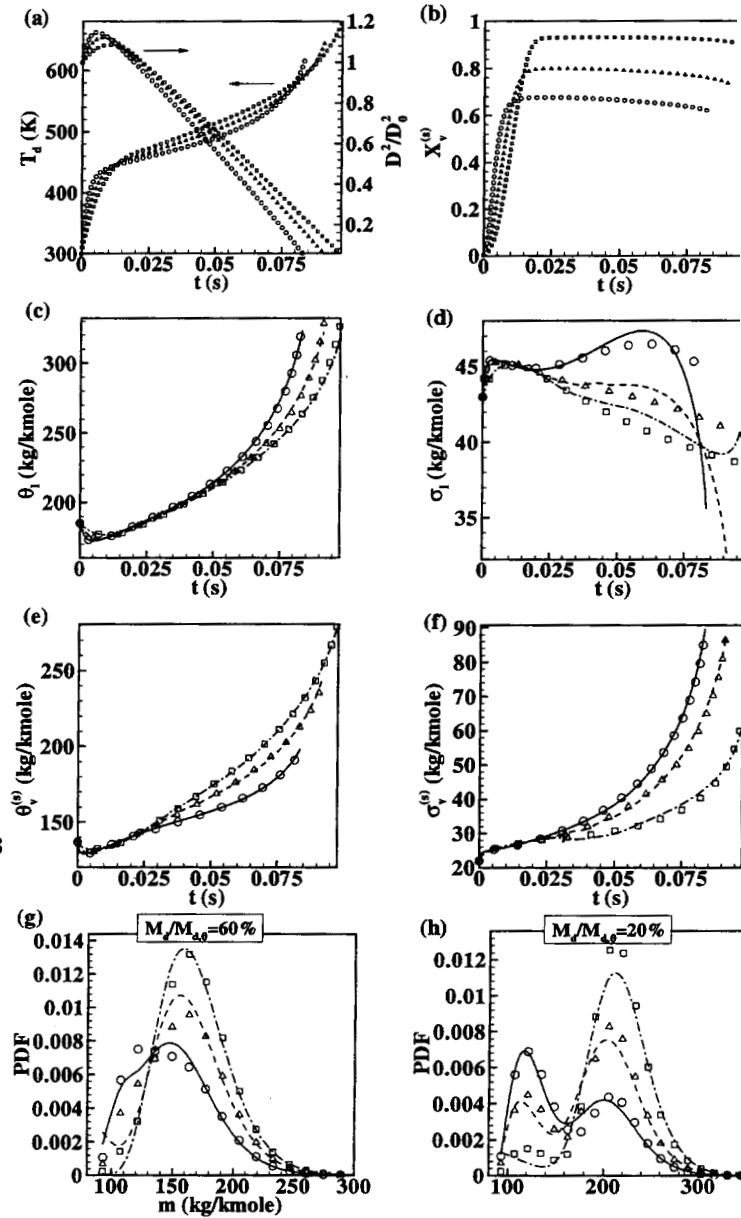


Figure 9: Drop history for Runs 2, 9 and 10 of Table 1: — and o for $Le = 0.5$, - - - and Δ for $Le = 1$ and - · - · and \square for $Le = 2$. Discrete (symbols) versus double- Γ -PDF (lines) model. (a) Drop temperature and relative surface area (discrete model only), (b) Drop surface vapor mole fraction (discrete model only), (c) Liquid mean molar weight, (d) Liquid PDF standard deviation, (e) Surface composition mean molar weight, (f) Surface composition PDF standard deviation, (g) Surface vapor PDFs at 60% residual drop mass, and (h) Surface vapor PDFs at 20% residual drop mass.